Characterization of Ozone Production in San Antonio, Texas Using Measurements of Total Peroxy Radicals

Daniel C. Anderson[1], Jessica Pavelec[1], Conner Daube[2], Scott C. Herndon[2], W. B. Knighton[3], Brian M. Lerner[2], J. Robert Roscioli[2], Tara I. Yacovitch[2], Ezra C. Wood[1]

[1]Department of Chemistry, Drexel University, Philadelphia, PA, USA

[2]Aerodyne Research Inc., Billerica, MA, USA

[3]Department of Chemistry and Biochemistry, Montana State University, Bozeman, MT, USA

Abstract

Observations of total peroxy radical concentrations ($[XO_2] \equiv [RO_2] + [HO_2]$) made by the Ethane CHemical AMPlifier (ECHAMP) and concomitant observations of additional trace gases made onboard the Aerodyne Mobile Laboratory (AML) during May 2017 were used to characterize ozone production at three sites in the San Antonio, Texas region. Median daytime $[O_3]$ was 48 ppbv at the site downwind of central San Antonio. Higher concentrations of NO and XO_2 at the downwind site also led to median daytime ozone production rates ($P(O_3)$) of 4.2 ppbv hr^{-1}, a factor of two higher than at the two upwind sites. The 95th percentile of $P(O_3)$ at the upwind site was 15.1 ppbv hr^{-1}, significantly lower than values observed in Houston. *In situ* observations, as well as satellite retrievals of HCHO and NO_2, suggest that the region was predominantly NO_X-limited. Only approximately 20% of observations were in the VOC-limited regime, predominantly before 11 am, when ozone production was low. Biogenic volatile organic compounds (VOC) comprised 55% of total OH reactivity at the downwind site, with alkanes and non-biogenic alkenes responsible for less than 10% of total OH reactivity in the afternoon, when ozone production was highest. To control ozone formation rates at the three study sites effectively, policy efforts should be directed at reducing NO_X emissions. Observations in the urban center of San Antonio are needed to determine whether this policy is true for the entire region.

1. Introduction

Tropospheric ozone (O_3) is a secondary air pollutant formed through a series of reactions involving volatile organic compounds (VOCs) and NO_X ($[NO_X] \equiv [NO] + [NO_2]$, where NO is nitric oxide and NO_2 is nitrogen dioxide). While tropospheric ozone exists naturally through stratospheric transport (Holton et al., 1995) and *in situ* tropospheric production, human activities have drastically perturbed these background values (Lamarque et al., 2005). Exposure to ozone adversely impacts human health, limiting lung and cardiac function, exacerbating chronic respiratory illnesses, and precipitating early mortality (Bell et al., 2006;Park et al., 2005;Jerrett et al., 2009;Silva et al., 2013). In response to these adverse impacts, in 2015 the United States Environmental Protection Agency (EPA) imposed an 8 hour ozone standard of 70 ppbv, lowering the exposure limit from the 75 ppbv standard set in 2008 (EPA, 2015). While ambient concentrations of the ozone precursor NO_X have declined significantly over much of the US (Choi and Souri, 2015;He et al., 2013;Duncan et al., 2016;Lamsal et al., 2015), reductions in ozone concentrations have been less dramatic. Background ozone concentrations have actually increased in some locations (Cooper et al., 2012;Choi and Souri, 2015); in other areas that have seen decreases in ambient ozone concentrations, such as Texas and the mid-Atlantic region, ozone still periodically exceeds the EPA standard (e.g. He et al., 2013).

Ozone production is generally classified as either NO_X- or VOC-limited (Kleinman, 1994;Thornton, 2002). Net formation of ozone occurs when NO is oxidized to NO_2 by reaction with the hydroperoxyl radical (HO_2) or an organic peroxy radical (RO_2). In the NO_X-limited regime, comparatively low concentrations of NO_X allow for the removal of RO_X radicals ($[RO_X] \equiv [OH] + [HO_2] + [RO_2]$, where OH is the hydroxyl radical) by self-reactions (e.g. Reactions R1 – R3). In the VOC-limited regime, RO_X radicals are removed from the atmosphere by reactions

with NO_X, producing less reactive compounds such as nitric acid (HNO_3) (Reactions R4 – R6). In the NO_X-limited regime, reductions in NO_X lead to reductions in O_3; while in the VOC-limited regime, reductions in NO_X without concomitant reductions in VOCs can actually increase O_3 production. One prominent example of this is the weekday/weekend effect in the Southern California Air Basin, where O_3 increases on weekends due to decreases in NO_X emissions from heavy duty diesel trucks (Pollack et al., 2012). The effective implementation of ozone reduction policies therefore requires a detailed understanding of the ozone production regime of the target area.

$$HO_2 + OH \rightarrow H_2O + O_2 \quad \text{(R1)}$$
$$HO_2 + HO_2 + M \rightarrow H_2O_2 + O_2 + M \quad \text{(R2)}$$
$$HO_2 + RO_2 \rightarrow ROOH + O_2 \quad \text{(R3)}$$
$$OH + NO_2 + M \rightarrow HNO_3 + M \quad \text{(R4)}$$
$$NO + RO_2 + M \rightarrow RONO_2 + M \quad \text{(R5)}$$
$$NO_2 + R(O)O_2 + M \rightarrow R(O)O_2NO_2 + M \quad \text{(R6)}$$

Texas is the second most populous state in the US. With multiple large urban centers and a mixture of urban and industrial emissions from petrochemical processing facilities as well as from natural gas and oil extraction, the state has complex pollution chemistry. This combination of a large population and pollution makes understanding ozone production in this region particularly important. Previous studies of ozone formation in Texas have focused primarily on Houston and the surrounding region. Mazzuca et al. (2016) used *in situ* observations of NO_X and O_3 from the DISCOVER-AQ campaign in summer 2013 along with output from the CMAQ model to find significant diurnal variability in ozone production, with higher ozone production rates ($P(O_3)$) in the morning and a transition from the VOC- to NO_X-limited regime before afternoon. Similar results were found during the TEXAQS2000, TRAMP2006, and SHARP 2009 campaigns (Mao et al., 2010;Ren et al., 2013). Multiple studies have found that anthropogenic alkenes, particularly ethylene and propylene, are major

contributors to OH reactivity and therefore O_3 production (Mao et al., 2010;Kleinman et al., 2002;Ryerson et al., 2003) in the region leading to $P(O_3)$ greater than 50 ppbv hr^{-1} (Mazzuca et al., 2016). OH reactivity is defined as the sum of the products of the concentration of species X and the reaction rate coefficient (k_{X+OH}) of X with OH (Eq. 1).

$$k_{OH} = \sum_i k_{(X+OH)}[X]_i \quad (1)$$

There have been comparatively few field campaigns, however, to study San Antonio, Texas, the seventh most populous city in the US. In July 2018, the EPA designated the San Antonio region as being in marginal non-attainment with the new 70 ppbv standard, suggesting a need to understand the O_3 formation chemistry in the region. In addition, San Antonio has a significantly different emissions profile than Houston. For example, examination of long-term VOC monitoring in Floresville, TX, a site immediately upwind of San Antonio, suggests that OH reactivity is dominated by alkanes (Schade and Roest, 2016) in contrast with the dominance of alkenes in Houston. Fig. 1 shows the trends in concentrations of ozone, NO_X, and O_X ($O_X \equiv O_3 + NO_2$) at two Texas Commission on Environmental Quality (TCEQ) monitoring sites, with one (Camp Bullis) located northwest of the urban center and the other (Pecan Valley) in the downtown area (Fig. 2b). With the lowering of the 8-hour ozone standard from 75 ppbv (dashed purple line) to 70 ppbv (solid purple line), the Camp Bullis site is much more likely to be in exceedance, while the Pecan Valley site remains below both standards. Despite noticeable decreases in maximum NO_X at both sites over the 14-year period shown here, there is little noticeable trend in ozone. This is in agreement with Choi and Souri (2015), who found a 0.07×10^{15} $cm^{-2}yr^{-1}$ decrease in tropospheric column NO_2 over San Antonio between the years 2005 and 2014 while finding an increasing trend of 0.64 ppbv yr^{-1} in the minimum value of surface

ozone over the same period. Further study is needed in the San Antonio region to understand the driving factors behind ozone production.

In this manuscript, we present results from the San Antonio Field Study (SAFS) conducted in the San Antonio, Texas region in May 2017. We show observations of total peroxy radical concentrations ($[XO_2] \equiv [RO_2] + [HO_2]$) from three sites in the San Antonio area, characterizing the XO_2 distribution in the region. We use these XO_2 measurements, along with observations of NO and other trace gas species, to quantify ozone production in regions up- and downwind of the urban core. Though there have been many prior determinations of $P(O_3)$ using measurements of a subset of peroxy radicals (*i.e.*, using laser-induced fluorescence measurements of HO_2 and a fraction of RO_2) (e.g. Ren et al., 2013), this is one of the few determinations of ozone production using the direct observation of total peroxy radicals (Sommariva et al., 2011). Combined with quantification of the primary production of RO_X radicals ($P(RO_X)$) and satellite retrievals of HCHO and NO_2, we determine the ozone production regime in San Antonio. Finally, we explore the main contributors to OH reactivity in the region.

2. Methodology

2.1 Campaign Description

The SAFS campaign was conducted from 11 to 31 May 2017 at several sites in the greater San Antonio region. We describe measurements made on the Aerodyne Mobile Laboratory (AML) at three sites: the University of Texas San Antonio (UTSA) from 11 to 16 May and from 27 to 31 May, Floresville, Texas from 16 to 21 May, and Lake Corpus Christi (Corpus) from 21 to 26 May. The sites were chosen to determine the impact of various emission sources on ozone formation affecting San Antonio. During May in southeastern Texas, the prevailing wind direction is southeasterly, coming off the Gulf of Mexico. UTSA is located

114 northwest (*i.e.* downwind) of downtown San Antonio (Fig. 2a) while the Floresville and Corpus
115 sites were both located upwind of the city. This allows for the determination of background
116 values of compounds through observation at the Floresville and Corpus sites, while observations
117 at UTSA are more representative of air photochemically processed with urban emissions. We
118 define background here as values upwind of the UTSA site. The AML was situated at all sites to
119 minimize influence from local emissions. At UTSA, the AML was located in a mostly vacant
120 parking lot about 1 km south of the nearest major roadway. In Floresville and Corpus, there
121 were no nearby major roadways, local traffic was at a minimum, and influence from local point
122 and mobile sources was limited. Potential influences from transient local sources (e.g. lawn
123 mowers and jet skis) were removed in the same manner as interference from the generator
124 emissions described below.

125 The AML is outfitted to measure a suite of gas- and particle-phase atmospheric species
126 (Herndon et al., 2005). All instrument inlets were mounted approximately 15 m above ground
127 level on a retractable tower located near the AML. At both the Floresville and UTSA sites, the
128 AML was powered through connection to the local electric utility while at Corpus a diesel
129 generator was used. Although the generator was situated downwind of the instrument inlets,
130 some stagnation and recirculation did occur, allowing for occasional sampling of generator
131 exhaust. Air parcels affected by the generator exhaust were removed through analysis of CO
132 observations. A filter for generator-influenced air was created by determining the minimum CO
133 value over a 100 s period every 5 minutes. Any air parcel with a CO mixing ratio 10 ppbv
134 higher than this minimum was assumed to be impacted by a local transient source, including the
135 generator.

Trace gases measured during SAFS and used in this study are summarized here. Unless otherwise indicated, data used in this study were reported as 1-minute averages and then averaged to the 2-minute Ethane CHemical AMPlifier (ECHAMP) time base, described in the following section. NO_2 was measured at 1 Hz via Cavity Attenuated Phase Shift (CAPS) spectroscopy (Kebabian et al., 2005;Kebabian et al., 2008). Nitric oxide (NO) was measured at 0.1 Hz through the same inlet as NO_2 and O_3 using a Thermo Fisher 42i-TL chemiluminescence analyzer, while O_3 was measured with a 2B-Tech model 205 ultraviolet (UV) absorption instrument. Uncertainties (2σ) of the NO, NO_2, and O_3 observations on the ECHAMP measurement time scale are below 5%. The above instruments were zeroed every 15 minutes with humidity-matched zero air. The zero air was generated by passing ambient air through an Aadco ZA30 Catalyst system for VOC removal and through Purafill Chemisorbant Media, a potassium permanganate based scrubber, for NOx removal.

Quantum Cascade – Tunable Infrared Laser Direct Absorption Spectrometers (QC-TILDAS) from Aerodyne Research Inc. (ARI) were used to measure CO and H_2O (2200 cm^{-1}; measurement wave number), HCHO (1765 cm^{-1}), CH_4 and C_2H_6 (2990 cm^{-1}), H_2O_2 (1277 cm^{-1}), and C_3H_8 (2965 cm^{-1}) (McManus et al., 2015). A Proton Transfer Reaction – High Resolution – Time of Flight (PTR-HR-ToF) mass spectrometer was used to measure isoprene, acetaldehyde, acetone, benzene, methanol, the sum of monoterpenes, the sum of methyl vinyl ketone (MVK) and methacrolein, and toluene. Typical measurement uncertainties were on the order of 25%. Finally, a prototype of a commercially-available gas chromatograph from ARI with electron-impact time-of-flight mass spectrometer (GC-EI-ToF-MS) was used to measure a suite of VOCs, including isoprene, 1,2,3-trimethylbenzene, ethyl benzene, cyclohexane, *n*-heptane, *n*-hexane, *n*-octane, *n*-pentane, *o*-xylene, and the sum of *m*- and *p*- xylenes. The GC

sampled with a multi-component adsorbent trap (Pollmann et al., 2006) for a 5 minute integration period every 20 minutes. GC observations are unavailable for 20-30 May. While toluene and *m*- and *p*- xylene measurement uncertainty was on the order of 20%, typical measurement uncertainties of other observed species, except isoprene, were on the order of 10%.

While there were two independent observations of isoprene, there were limitations with both methods. It was determined that the actual isoprene concentration in the calibration standard used in the field for the PTR had degraded over time, resulting in erroneously high isoprene values. On the other hand, the GC was not calibrated for isoprene during the campaign and observations are only available for half the time. As a result, we use the PTR isoprene from the entire campaign scaled to the GC values, using a GC isoprene sensitivity determined after the campaign. This method results in an estimated isoprene uncertainty of ≈30% (1σ). See the SI for more information.

Temperature, wind speed, and wind direction were measured at the top of the inlet tower with a 3D RMYoung (Model 81000RE) sonic anemometer. Atmospheric pressure observations used in this study were taken from the National Weather Service observations at the San Antonio International Airport for the UTSA and Floresville sites and from the Corpus Christi International Airport for the Corpus site. NO_2 photolysis frequencies (J_{NO2}) were measured via a filter radiometer (MetCon, GmbH) located on top of the AML (Shetter et al., 2003;Stark et al., 2007).

2.2 ECHAMP

Total peroxy radical concentrations ([XO_2]) were measured via chemical amplification by the ECHAMP instrument. A complete instrument description can be found in Wood et al. (2017), and only the most relevant details are summarized here, including a new sampling

system that includes an integrated, remotely-controlled RO_X calibration source. Briefly, ECHAMP measures total XO_2 concentration at a two-minute resolution by reacting peroxy radicals with excess NO and ethane (C_2H_6). Through a series of chain reactions, each XO_2 radical produces approximately 20 NO_2 molecules (depending on the relative humidity (RH)), which are then measured with a commercially available NO_2 monitor. Because this NO_2 monitor also measures ambient O_3 and NO_2 (O_X), a second channel and dedicated NO_2 monitor are used to only measure the sum of [O_3] and [NO_2]. The difference between the two channels, divided by the "amplification factor" of ≈20, yields the XO_2 concentration.

The inlet box is a 39 cm × 44 cm × 16 cm fiberglass, rainproof electrical enclosure. The box was mounted at the top of the sampling tower and connected to the rest of the instrument via a bundle of tubes and electrical cables. Ambient air was sampled at a flow rate of 6.5 LPM through 76 mm of 3.6 mm inner diameter (ID) glass into the inlet box (see Fig. S1 for a schematic of the plumbing). The glass was internally coated with halocarbon wax to minimize wall losses of XO_2. The flow was sub-sampled into two, 1.9 cm^3 reaction chambers at a flow rate of 1.1 LPM each. Temperature and RH of the remaining 4.5 LPM of sampled air were measured with a Vaisala probe (Model HMP60). Laboratory tests over a range of flow rates and RH have demonstrated sampling losses of HO_2 of less than 3% and negligible losses of CH_3O_2 (Kundu et al., 2019).

Reaction chambers cycled every minute between an amplification mode and a background mode, for a total cycle time of 2 minutes. In both modes, 25 sccm of 39.3 ppmv NO in N_2 (Praxair) was added at the beginning of the reaction chamber, resulting in a final NO mixing ratio of 0.90 ppmv. In amplification mode, 35 sccm of a 42.2% ethane mixture in N_2 (Praxair) was also added to the sampled air at the beginning of the reaction chamber. The radical

propagation scheme shown in reactions R7 – R13, in which Reactions (R9) – (R13) repeat numerous times, results in formation of NO_2. The number of NO_2 molecules formed per XO_2 molecule sampled is known as the amplification factor (F) and varies with RH. During SAFS, F was 23 for dry air and decreased to 12 at 58% RH. The two calibration methods used to determine F are described below and more fully in the SI. At 15.2 cm downstream of the NO/C_2H_6 injection point, 35 sccm of N_2 was added to the flow. In the background chamber, the N_2 and C_2H_6 flows were switched (N_2 was added upstream, and C_2H_6 was added downstream), allowing XO_2 radicals to react with NO to form HONO or alkyl nitrates before 35 sccm of the 42.2% ethane mixture was added at the end of the reaction chamber. The resultant NO_2 from each chamber was then measured with separate, dedicated CAPS instruments. Total XO_2 was then determined by the difference between the two NO_2 measurements divided by F.

$$RO_2 + NO \rightarrow RO + NO_2 \quad \text{(R7)}$$
$$RO \rightarrow HO_2 + \text{products} \quad \text{(R8)}$$
$$HO_2 + NO \rightarrow OH + NO_2 \quad \text{(R9)}$$
$$OH + C_2H_6 \rightarrow H_2O + C_2H_5 \quad \text{(R10)}$$
$$C_2H_5 + O_2 + M \rightarrow C_2H_5O_2 + M \quad \text{(R11)}$$
$$C_2H_5O_2 + NO \rightarrow C_2H_5O + NO_2 \quad \text{(R12)}$$
$$C_2H_5O + O_2 \rightarrow CH_3CHO + HO_2 \quad \text{(R13)}$$

The CAPS instruments were calibrated for NO_2 before, after, and once during deployment via quantitative reaction of known concentrations of O_3 generated with a 2B Technologies ozone generator (Model 306) with excess NO. This ozone source agreed within 1% with a separate Thermo ozone generation source (Model 49C). All NO_2 calibrations agreed within 5%. The amplification factor (F) was determined by producing known amounts of peroxy radicals by two calibration methods: photolysis of H_2O and of CH_3I. Both methods are described in more detail in the SI. Briefly, the H_2O photolysis method is similar to that used by most HO_X instruments, in which H_2O was photolyzed at a wavelength of 184.9 nm to form an equimolar

mixture of OH and HO_2 (Mihele and Hastie, 2000;Faloona et al., 2004). This mixture was then reacted with H_2 to convert the OH into HO_2. Radical concentrations were quantified using the relevant spectroscopic parameters and the measured H_2O and O_3 concentrations in the calibration gas.

The second calibration method was based on 254 nm photolysis of CH_3I in humidified air, producing the CH_3O_2 radical. The radical concentration is quantified by reaction of the CH_3O_2 with NO in the absence of C_2H_6, producing 1.86 NO_2 molecules per CH_3O_2. The H_2O photolysis method was performed 6 times, while the CH_3I method was performed once during the field campaign, on 31 May. Both methods were repeated twice in the laboratory after the campaign. Observations from ECHAMP agreed within 12% with the H_2O photolysis calibration source operated by Indiana University during a comparison study in 2015 (Kundu et al., 2019). For the XO_2 observations described in this paper, we use the CH_3I calibration. While both methods agree within uncertainty, the H_2O photolysis method was only conducted for RH values of less than approximately 20%, much lower than typical ambient RH. See the SI for further information.

The total 2σ accuracy for XO_2 during SAFS was approximately 25%. Calibrations were not performed at RH values greater than 71%. Therefore, we omit all observations with a sample RH greater than 71%. Approximately 85% of these high RH points were observed at nighttime, so we only consider daytime data (7:00 – 20:00 local time) unless otherwise indicated.

2.3 Calculation of $P(O_3)$ and $P(RO_X)$

We use measurements of XO_2 and NO to calculate the gross rate of ozone production $P(O_3)$ using Eq. (2), in which k_{NO+HO2} is the reaction constant for the reaction of NO with HO_2 and k_i is the reaction constant for NO with an organic peroxy radical $[RO_2]_i$. We note that this is

more accurately described as the rate of odd oxygen (O_X) production. Because ECHAMP only measures the sum of peroxy radicals and not their speciation, we assume a simplified form of this relationship (Eq. 3), where k_{eff} is an effective rate constant taken as that of k_{NO+HO2}. Box modeling results for this site, which will be discussed more fully in a forthcoming paper, show the dominant XO_2 species are HO_2, CH_3O_2, and isoprene RO_2. At 298 K, k_{NO+HO2} is within 10% of the k values for the reaction of NO with CH_3O_2 and isoprene RO_2 (Orlando and Tyndall, 2012), supporting our choice of k_{eff}. Further, while the reaction of NO with acetyl peroxy radicals is approximately 2.5 times faster than with other peroxy radicals at 298K, box modeling results suggest that these radicals comprise only 5 – 10% of total XO_2, resulting in an average difference in $P(O_3)$ of 15% from the k_{NO+HO2} value used here. This uncertainty is comparable to the total uncertainty of the k_{NO+HO2} rate constant, estimated as 15% (Sanders et al., 2011). As will be shown in Section 3.2, our conclusions are insensitive to the value of k_{eff} chosen. Uncertainty in gross $P(O_3)$ results from uncertainty in the NO and XO_2 measurements, 5% and 25%, respectively, and k_{eff}, whose uncertainty we estimate at 23%, determined by adding the uncertainty in the k_{NO+HO2} rate constant and the uncertainty in the choice of k_{eff} in quadrature. This results in a total $P(O_3)$ uncertainty of 34%.

$$P(O_3)_{Gross} = k_{NO+HO2}[NO][HO_2] + [NO]\sum_i k_i[RO_2]_i \quad (2)$$

$$P(O_3)_{Gross.} = k_{eff}[NO][XO_2] \quad (3)$$

$$L(O_3) = \left(\frac{k_{O1D+H2O}[H_2O]}{k_{O1D+H2O}[H_2O] + k_{O1D+N2}[N_2] + k_{O1D+O2}[O_2]} J_{O1D} + k_{OH+O3}[OH] + k_{HO2+O3}[HO_2] + \sum_i k_{alkene-i}[alkene_i]\right)[O_3] + k_{OH+NO2}[OH][NO_2][M] \quad (4)$$

The net formation rate of O_3 is equal to $P(O_3)_{Gross} - L(O_3)$. In order to tie $P(O_3)$ completely to observations, we report only gross $P(O_3)$, not net $P(O_3)$. That is, we only calculate the production term (Eq. 2) and not the loss term (Eq. 4) for net ozone production. Calculation of the loss term requires knowledge of the concentration of OH and alkenes as well as the fraction of total XO_2 comprised of HO_2. Of these quantities, only a small subset of alkenes - isoprene and monoterpenes - were measured during SAFS. Estimating the alkene loss term using concentrations from nearby TCEQ monitoring sites, suggests that O_3 loss due to this pathway is negligible for the data analyzed here, and we omit this from our calculation of ozone loss. To estimate OH and the fraction of XO_2 comprised of HO_2 and to determine whether analyzing only gross $P(O_3)$ affects our conclusions, we used the Framework for 0-Dimensional Atmospheric Modeling (F0AM) box model (Wolfe et al., 2016b) to calculate OH and the fraction of RO_2 comprised of HO_2. A description of the model setup can be found in the SI. For data points that were not modeled due to missing model constraints, these values were estimated from interpolation of modeled values, if observations were made within two hours of a modeled data point, or from site-specific mean daily profiles if no modeled points were available. Using these modeled-derived values for OH and the HO_2 fraction, median $L(O_3)$ for daytime observations at all sites were determined to be 0.90 ppbv/hr, which is 16% of the gross production rate.

We use Eq. (5) to calculate the primary RO_X production rate. Here, $P(RO_X)$ is the RO_X production rate, J indicates photolysis rate, and $k_{O1D+H2O}$, k_{O1D+O2}, and k_{O1D+N2} are the reaction rate constants for the reaction of O_{1D} with the indicated species. The Tropospheric Ultraviolet and Visible (TUV) model was used to calculate photolysis rate constants (J values), which were then scaled to the measured J_{NO2}. HONO was not measured during SAFS. We estimate HONO

concentrations assuming an upper limit to the [HONO]/[NO_X] ratio of 0.04 as described in Lee et al. (2013). This is an upper bound on the HONO concentration and thus on HONO contribution to P(RO_X). Alkene concentrations were estimated from nearby TCEQ monitoring sites, as described in Sect. 3.3. Alkene ozonolysis was calculated to have a negligible impact on P(RO_X) and is omitted from the analysis.

$$P(RO_X) = 2J_{O1D}[O_3]\frac{k_{O1D+H2O}[H_2O]}{k_{O1D+H2O}[H_2O]+k_{O1D+N2}[N_2]+k_{O1D+O2}[O_2]} + 2J_{HCHO}[HCHO] + 2J_{CH3CHO}[CH_3CHO] + 2J_{Acetone}[CH_3COCH_3] + 2J_{H2O2}[H_2O_2] + J_{HONO}[HONO] \quad (5)$$

Total P(RO_X) peaks at midday at about 0.65 pptv s^{-1} on average and is dominated by the ozone and HCHO terms, terms 1 and 2 from Eq. (5), respectively, with contributions from the other observed species totaling less than 5% on average. Contributions from HONO were generally less than 0.1 pptv s^{-1}, even assuming the upper bound in the HONO to NO_X ratio used here.

2.4 Satellite Data

We use observations of NO_2 and HCHO from the Ozone Monitoring Instrument (OMI) to provide a remotely-sensed estimate of the surface ozone production regime in San Antonio (Duncan et al., 2010;Ring et al., 2018). OMI has a local overpass time of about 13:30 and provides daily, global coverage. The instrument measures backscattered solar radiation in the UV/visible region, allowing for differential optical absorption spectroscopy (DOAS) type retrievals of multiple species, including NO_2 and HCHO.

For NO_2, we use the NASA Goddard Space Flight Center (GSFC) version 3 level 2 tropospheric column product (Bucsela et al., 2013;Krotkov et al., 2017) gridded to 0.25º latitude × 0.25º longitude resolution. For HCHO, we use the version 3 level 2 reference sector corrected swath product from the Harvard-Smithsonian Astrophysical Observatory (SAO) retrieval (González Abad et al., 2015) also on a 0.25º latitude × 0.25º longitude grid. For both OMI

products, we use only pixels that satisfy quality and row anomaly flags, have a cloud fraction less than 30%, and a solar zenith angle less than 70º. Additionally, data from the two outer most pixels are removed due to their large footprint (28km × 150km) compared to the nadir view.

We analyze the HCHO to NO_2 ratio using OMI data from May to July 2017. While SAFS lasted only one month, missing data due to cloud cover, the row anomaly, and other factors necessitate a longer time period for data averaging. To calculate the ratio of HCHO to NO_2, we first calculate the standard deviations (σ) of the HCHO and NO_2 data at each grid point. When calculating the ratio, we only include days within 2σ of the average HCHO and NO_2 observations and only include grid boxes that have at least 10 days with coincident observations of both species.

3. Results

3.1 Distribution of Ozone and its precursors

The highest ozone mixing ratios observed at UTSA were on 14 and 15 May, reaching a maximum near 80 ppbv, while daytime values typically varied between 40 and 60 ppbv during the remainder of the campaign (Fig. 3). Median daytime [O_3] at all three measurement sites was 37 ppbv (Fig. 4a). Median ozone was 18 ppbv higher at UTSA than at the background site in Floresville. Although the highest ozone values were seen at UTSA, there was significant overlap in the ozone distribution between the UTSA and Corpus sites. Consistent with the higher O_3 abundance, concentrations of the O_3 precursors isoprene, NO, and XO_2 were also highest at the UTSA site. Median isoprene concentrations, one of the largest contributors to OH reactivity as will be shown later, was almost two orders of magnitude larger at UTSA (1.2 ppbv) than at the other sites (0.05 and 0.03 ppbv at Floresville and Corpus, respectively). While the difference in median [NO] at the sites was not as extreme, a much larger range was seen at UTSA, where the

95th percentile of observations was above 2 ppbv. Similar results are seen for the [XO_2] distribution (Fig. 4c), with the highest XO_2 mixing ratios (90 pptv) coinciding with the maximum O_3. Median [XO_2] was approximately 1.5 times higher at the UTSA site (37 pptv) than at Floresville (26 pptv) and Corpus (25 pptv).

XO_2 concentrations showed a distinct diurnal profile (Fig. 5). Overnight values were approximately constant with a median of around 10 pptv, until a small decline after 3:00. A steady increase in [XO_2] began at 9:00, with a peak of 50 pptv at 15:00 and then a decline to the overnight value by 20:00. The shape of this profile is in agreement with other observations of peroxy radicals from a variety of chemical environments (Sanchez et al., 2016;Mao et al., 2010;Whalley et al., 2018). Noise in the nighttime data is a result of higher RH and thus degraded precision of the ECHAMP measurement technique and is not an indication of significant nighttime variability. Even though we have filtered for data points with RH greater than 71% as discussed in Sect. 2.2, nighttime RH is higher than daytime values, on average, decreasing measurement precision. Daytime variability resulted from changes in insolation and biogenic VOC concentrations. The days that showed little or no diurnal profile at UTSA and Corpus were overcast, as evidenced by low J_{NO2} (Fig. 3). Concentrations of isoprene and the sum of methyl vinyl ketone (MVK) and methacrolein, both isoprene degradation products, were at a maximum when [XO_2] peaked at 90 pptv.

The higher O_3 concentrations at UTSA are consistent with its location downwind of the urban core of San Antonio. Figure S2 shows wind roses colored by ozone and the ozone precursors described above. The wind direction while at UTSA was predominantly southeasterly, in agreement with the climatological average for the region. The highest ozone mixing ratios, as well as the highest XO_2 and isoprene, were seen when air parcels originated

from this direction, travelling over the city. The highest [NO] (greater than 2.2 ppbv), however, was seen with northerly and northeasterly winds. This is likely because of the proximity of a major highway north of the UTSA site, which would provide a source of recently-emitted, less processed emissions than in air parcels that travelled from downtown San Antonio. The CO distribution by wind direction (not shown) is consistent with this explanation.

3.2 Ozone production

The highest $P(O_3)$ values (and highest [NO] and $[XO_2]$) were observed at UTSA. Median $P(O_3)$ between 7:00 and 20:00 at UTSA was 4.1 ppbv hr^{-1}, compared to just over 1 ppbv hr^{-1} at both Floresville and Corpus. The 95th percentile, 12.6 ppbv hr^{-1}, is significantly lower than rates found in Houston, which frequently topped 40 ppbv hr^{-1} (Mazzuca et al., 2016;Mao et al., 2010). As with $[O_3]$ and $[XO_2]$, the highest $P(O_3)$ rates occurred when winds travelled over downtown San Antonio.

Figure 6a shows the variation in $P(O_3)$ with [NO], where the data points have been colored by $P(RO_X)$ for all observations taken during SAFS. The relationship for the subset of observations exclusively at UTSA is essentially identical. In general, $P(O_3)$ increases with [NO], although a wide range of $P(O_3)$ exists for a given value of NO. For a constant value of [NO], $P(O_3)$ is consistently higher at higher $P(RO_X)$. Figure 6b shows the same data as panel 6a but binned both by NO mixing ratio and $P(RO_X)$. All $P(O_3)$ observations have been separated into NO bins with an equal number of observations, as well as into two bins of $P(RO_X)<0.2$ and $P(RO_X)>0.4$. The values of $P(RO_X)$ were chosen to represent the low and high ranges of $P(RO_X)$ observed during SAFS. The conclusions drawn from the results are insensitive to the values chosen for these bins.

Figure 6b demonstrates that the majority of observations made during SAFS were in the NO_X-limited regime. For the high $P(RO_X)$ observations, there is a steady increase in $P(O_3)$ up to

379 the 500 pptv NO bin. Above this point, $P(O_3)$ potentially plateaus, but there were insufficient
380 observations at higher NO to determine the location of the turnover point in ozone production.
381 Because the majority of NO observations at UTSA were less than 500 pptv, we conclude that the
382 site is predominantly NO_X-limited. Further observations at higher NO mixing ratios are required
383 to determine the turnover point for ozone production in this region. The true turnover
384 concentration for NO cannot be easily inferred by inspection of a graph of $P(O_3)$ versus [NO],
385 however, because VOC concentrations are not constant for all points. To see if there is any
386 variation in this relationship with VOCs, we further separate the high $P(RO_X)$ data by their VOC
387 reactivity (Fig. S3). VOC reactivity (VOCR) was calculated in the same manner as OH
388 reactivity, described in section 3.3, but including only OH reactive VOCs. In addition, VOCs
389 exclusively observed by the GC instrument were not included in the calculation as they were
390 only available until 19 May. For data points with GC observations available, VOC reactivity
391 increased by only 2% in the afternoon and 12% in the morning on average when including the
392 GC observations, suggesting that this omission does not significantly affect the results. Data
393 were then separated into low ($VOCR < 3\ s^{-1}$), medium ($3\ s^{-1} < VOCR < 6\ s^{-1}$), and high ($6\ s^{-1} <$
394 $VOCR < 9\ s^{-1}$) VOC reactivity bins. For the high $P(RO_X)$ case, the relationship is similar for all
395 VOC reactivities, showing a general increase in $P(O_3)$ with NO, further suggesting the majority
396 of observations were NO_X-limited for high $P(RO_X)$. We note that for a constant $P(RO_X)$ value,
397 theoretically $P(O_3)$ is expected to increase with [NO] at approximately the same rate until the
398 turn-over point with little sensitivity to the VOC reactivity. The 5^{th} and 95^{th} percentiles of
399 $P(RO_X)$ for the high $P(RO_X)$ are 0.42 and 0.92 pptv s^{-1}, more than a factor of two different. This
400 suggests that the differences in the rate of change of $P(O_3)$ with NO for the different VOC
401 reactivities likely results from the wide range of $P(RO_X)$ values analyzed.

When looking at all points for the low $P(RO_X)$ case (Fig. 6b), there is a small peak in $P(O_3)$ at 200 pptv NO, suggesting that in a low $P(RO_X)$ environment, UTSA can be VOC-limited at higher NO mixing ratios. Separating these data points by VOC reactivity, shows more clearly the transition between the NO_X- and VOC-limited regimes. For the medium case, $P(O_3)$ first increases with [NO], peaks at 5 ppbv hr^{-1} at approximately 200 pptv [NO], and then declines to 2 ppbv hr^{-1} at 400 pptv [NO]. This peak and decline suggests that, for $P(RO_X) < 0.2$ pptv/s, VOC reactivities $< 6\ s^{-1}$, and NO > 200 pptv, the region is VOC-limited. For NO > 400 pptv, there is a slight increase in $P(O_3)$ with [NO], although the spread of data for a given [NO], also increases. For the low VOC reactivity scenario, the range of $P(O_3)$ for a given [NO] is also large compared to the mean $P(O_3)$, making it difficult to determine whether these points obey a similar relationship. As with the high $P(RO_X)$ scenario, each bin has a wide range of $P(RO_X)$ and VOC reactivities, which could lead to the large spread in data, suggesting the need for further observations. Separating the results by location yields the same results, although VOC reactivity at Floresville and Corpus were almost always below $3\ s^{-1}$ due to the lower isoprene concentration at these sites in comparison to UTSA.

Ozone production rates in VOC-limited regime are typically below 5 ppbv hr^{-1} and constitute only 20% of the observations examined here, suggesting that the all three SAFS sites are predominantly NO_X-limited. The majority of the VOC-limited points here (75%) occur before 11 EDT, when NO concentrations are higher and isoprene emissions and VOC reactivity are low. This is in agreement with the L_n/Q diurnal profile discussed below. For the NO_X-limited points, increases in VOC concentrations are expected to have a small impact on $P(O_3)$; for the VOC-limited points, increases in VOCs will lead to increased $P(O_3)$.

Finally, the results presented here are insensitive to the value of k_{eff} chosen. Figure S4 shows the relationship between $P(O_3)$ and NO for four different values of k_{eff}: k_{NO+HO2} (the k_{eff} used in this analysis), $k_{NO+CH3O2}$, $k_{NO+IsopreneRO2}$, and assuming $k_{NO+acetyl\ peroxy}$ for 10% of the value and k_{NO+HO2} for the remainder. While the magnitude of $P(O_3)$ does change with k_{eff}, the overall relationship is the same. As mentioned previously, the uncertainty in k_{NO+HO2} is larger than the uncertainty induced by the choice of k_{eff}. Additional analysis further suggests that the majority of the observations during SAFS were in the NO_X-limited regime.

These results are consistent with the diurnal profile of the ozone production regime as determined by the separate "L_N/Q" metric, which is the ratio of the RO_X loss rate due to reactions with NO_X (e.g., R3) to the total RO_X loss rate (Q) (Kleinman, 2005). In general, when more than half of the RO_X loss is due to reaction with NO_X species ($L_N/Q > 0.5$) then $P(O_3)$ is VOC-limited, whereas when the majority of RO_X loss is due to peroxy radical self-reactions ($L_N/Q < 0.5$) $P(O_3)$ is NO_X-limited. The Framework for 0-Dimensional Atmospheric Modeling (F0AM) photochemical box model (Wolfe et al., 2016b), constrained to observations, was used to model the parameters needed to calculate L_N/Q at the SAFS sites. A full description of the model setup is in the SI. Using the box model results and the method described in Kleinman (2005), we calculated L_N/Q for all box-modeled observations at UTSA (Fig. 7). A clear diurnal pattern is evident with an early morning maximum and then a quick decline to $L_N/Q < 0.5$ at 9:00, after which the ratio remains below 0.1 for the remainder of the day. At 18:00, however, the ratio does begin to increase, though remaining well in the NO_X-limited space. While L_N/Q is highest in the morning, $P(O_3)$ is at a minimum during this time period, suggesting that there is little O_3 production when $P(O_3)$ is VOC-limited. Furthermore, time periods where ozone was found under VOC-limited conditions were likely confined to a relatively small volume of air in the

shallow, morning boundary layer. This transition from VOC- to NO_X-limited between morning and afternoon is consistent with other locations (Mazzuca et al., 2016;Mao et al., 2010;Ren et al., 2013) and the high NO concentrations that build up in the morning from local traffic and a low boundary layer.

Finally, remotely sensed observations of NO_2 and HCHO from the OMI satellite corroborate the conclusion that ozone production in San Antonio is NO_X-limited. The ratio of column HCHO to tropospheric column NO_2 has been used as an indicator of the ozone production regime in multiple regions (Duncan et al., 2010;Ring et al., 2018). According to Duncan et al. (2010), a region is considered NO_X-limited when this ratio is greater than 2, VOC-limited for values less than 1, and in a transition region for ratios between 1 and 2. Other studies dispute these ranges, claiming that, in Houston, the NO_X-limited regime only begins for a ratio greater than 5 (Schroeder et al., 2017). Figure 2 shows the ratio averaged over the months May – July 2017 over Texas. In agreement with the *in situ* observations and the above analysis, the satellite data places all three locations in the NO_X-limited regime with ratios much greater than 5. Though they provide much higher spatial coverage, polar orbiting satellite observations are limited in that they provide coverage once daily and that data must be averaged over a long period to gain meaningful statistics. Likewise, because of the satellite footprint, any small regions in urban centers that may be VOC-limited might not be evident here because of spatial averaging. Nevertheless, the combination of satellite and *in situ* observations clearly demonstrates that, at least at the three measurement sites, ozone production was NO_X-limited.

3.3 OH Reactivity

In contrast with Houston, the OH reactivity, and thus ozone production, at the UTSA measurement site was driven by biogenic species, particularly isoprene. Figure 8 shows the OH reactivity for the UTSA and Floresville sites. Observations after 19 May were excluded because

471 of the lack of GC observations. Concentrations of all observed OH reactive species were used to
472 calculate the total OH reactivity. These values were then divided into several groups: biogenics
473 (isoprene, MVK, methacrolein, and α-pinene), carbonyls (HCHO and acetaldehyde), alkanes
474 (ethane, propane, cyclohexane, octane, heptane, hexane, and pentane), NO_X, CO, CH_4, O_3, and
475 other (benzene, 1,2,4-trimethylbenzene, ethyl benzene, toluene, *o*-, *p*-, and *m*-xylene, methanol,
476 and C_2H_2).

477 OH reactivity varied substantially at the two sites in both magnitude and relative
478 importance of the individual constituents. Overall, average afternoon OH reactivity at UTSA
479 and Floresville were 12 and 4.0 s^{-1}, respectively. While the main contributors to OH reactivity
480 varied between morning and afternoon at both sites, the total reactivity did not show significant
481 variation. The higher OH reactivity at UTSA is consistent with the higher $P(O_3)$ rate and XO_2
482 concentrations. At UTSA, the predominant contributors to OH reactivity were NO_X in the
483 morning and biogenic VOCs in the afternoon, comprising 46% and 55% of OH reactivity,
484 respectively. Isoprene dominated the biogenic contribution, with less than 10% of total OH
485 reactivity resulting from monoterpenes, which have been assumed to be 100% α-pinene.
486 Although the contribution of biogenic VOCs was lower at Floresville than at UTSA, they were
487 still the largest component of OH reactivity in the afternoon. The significant contribution to OH
488 reactivity from NO_X during the morning is consistent with large on-road emissions and a low
489 boundary layer as well as with the VOC-limited nature of O_3 production in the morning. During
490 these morning hours, when the region is VOC-limited and $P(RO_X)$ is generally less than 0.2
491 pptv/s, NO can frequently exceed 500 pptv (Fig. 6c), as compared to the campaign median of
492 225 pptv. CO and carbonyls were the other major contributors to OH reactivity at all locations,
493 with CO being the dominant contributor at Floresville in the morning. Because one of the

494 dominant contributors to HCHO production is isoprene (Wolfe et al., 2016a), it is likely that the
495 biogenic contribution to OH reactivity is even higher than indicated here. Contributions from
496 alkanes were unimportant at the UTSA site, 1% or less during both morning and afternoon, and
497 contributed only 4-5% at Floresville.

498 The uncertainty in the isoprene measurements does not significantly alter the conclusions
499 presented here. To bound the effect of this uncertainty, we adjusted the isoprene observations by
500 ± 32% and recalculated the OH reactivity. This results in a range of 10.5 – 13.4 and 3.8 – 4.3
501 s^{-1} in total afternoon OH reactivity at UTSA and Floresville, respectively. NO_X remains the
502 dominant contributor at UTSA in the morning. For the lower bound, isoprene contributes 49%
503 of total OH reactivity at UTSA, by far the largest contributor to afternoon OH reactivity, and
504 23% at Floresville, making it second in importance to CO (25%).

505 Because of the large contribution of alkenes to OH reactivity at other Texas sites (Mao et
506 al., 2010), it is necessary to make an estimate of their importance during SAFS. With the
507 exception of isoprene and monoterpenes, alkenes were not measured onboard the AML and
508 therefore have not been included in the above analysis. To estimate the impact of anthropogenic
509 alkenes on OH reactivity, we include in our calculation of OH reactivity observations of alkenes
510 made at nearby TCEQ monitoring sites, Camp Bullis for UTSA and a site in Floresville co-
511 located with the AML. These sites provide hourly observations of cis-2-butene, trans-2-butene,
512 1-pentene, cis-2-pentene, trans-2-pentene, ethene, propene, 1,3-butadiene, and 1-butene. Alkene
513 concentrations at the SAFS monitoring sites were assumed to be identical to those at the TCEQ
514 monitoring sites and were interpolated to the ECHAMP time base. This assumption is likely
515 more accurate for the Floresville site than for UTSA. A regression of hourly averaged *n*-pentane
516 measured onboard the AML to that measured at the Camp Bullis TCEQ site has an r^2 of 0.3,

517 even after maximizing the correlation using a lead-lag analysis. In addition, the maximum *n*-
518 pentane concentrations at the Camp Bullis site are almost a factor of 2 higher than those seen at
519 UTSA. Regressions of cyclohexane and benzene between the two sites show even lower r^2
520 values. On the other hand, a similar regression of n-pentane at the Floresville site has an r^2 of
521 0.83. Better agreement at Floresville is to be expected since the AML and TCEQ monitor were
522 co-located. Total OH reactivity was then recalculated using the estimates of alkene
523 concentrations. Alkenes contribute less than 1% of total reactivity at both UTSA and Floresville
524 for morning and afternoon times.

525 ***4. Discussion and conclusions***

526 We have presented observations of O_3, its precursors, and total observations of XO_2 at
527 three sites in the San Antonio region. We also presented determinations of $P(O_3)$ calculated from
528 measurements of total peroxy radicals. Median daytime $P(O_3)$ at UTSA was 4.1 ppbv hr^{-1},
529 compared to just over 1 ppbv hr^{-1} at the other two SAFS sites. Ozone production rates at UTSA
530 were still far lower, however, than values observed during campaigns in Houston. Mazzuca et
531 al. (2016) found median near surface gross $P(O_3)$ of about 10 ppbv hr^{-1} during the DISCOVER-
532 AQ campaign in the summer of 2013, with values up to 140 ppbv hr^{-1} seen over the Houston
533 shipping channel. These values are consistent with previous studies in the region (Sommariva et
534 al., 2011). Higher concentrations of NO and larger production rates of RO_X were seen during
535 DISCOVER-AQ than during SAFS, both of which could lead to higher $P(O_3)$.

536 During SAFS, ozone peaked at UTSA at 80 ppbv, with a median value of 47 ppbv,
537 almost 20 ppbv higher than at the background site of Floresville, upwind of San Antonio. Along
538 with higher O_3, the UTSA site also had larger $P(O_3)$, isoprene, NO, and XO_2 concentrations than
539 upwind sites. Differences in $[O_3]$ between the up- and downwind sites could be the result of the

effects of urban emissions on O_3 production, or they could result from daily variability, since simultaneous observations were not made at both sites and there are no permanent O_3 observations at Floresville. Figure S5 compares O_3 observations from the AML while at UTSA to those made by the University of Houston (UH), who measured O_3 continuously at UTSA during SAFS, and to observations from the TCEQ sites at Lake Calaveras, located upwind of downtown San Antonio (Fig. 2b), and Pecan Valley, situated in downtown San Antonio. Between 17 and 30 May, winds in the San Antonio region were primarily southeasterly (*i.e.* they travelled in the general direction from Lake Calaveras to UTSA, with downtown San Antonio in-between). During this period, there are both days where O_3 is almost identical at all sites and where O_3 is 20 ppbv higher at UTSA than at Lake Calaveras, suggesting significant O_3 production in the air as it travelled between the two sites. These results suggest that the 20 ppbv differences in median values between the UTSA and Floresville sites could be either the result of day-to-day variability, *in situ* O_3 production as the air travelled between the two sites, or a mixture of the two. Further observations of O_3 and its precursors in the region, including in downtown San Antonio, are needed to fully characterize the effects of the city on ozone production. In addition, future modeling studies will investigate the evolution of ozone production during this campaign.

A variety of methods were used to show that with the exception of early morning, when NO is high and XO_2 concentrations are low due to limited insolation, ozone production at the three SAFS sites is NO_X-limited. The relationship between $P(O_3)$ and NO was consistent at the three sites, although the lower $P(RO_X)$, NO, and VOC reactivity at Floresville and Corpus Christi led to overall lower ozone production rates as compared to UTSA. VOC-limited points comprised only 20% of total daytime observations and generally had $P(O_3)$ less than 5 ppbv hr^{-1}

563 at UTSA and less than 2 ppbv hr^{-1} at the other two sites. This diurnal cycle is in agreement with
564 observations made in Houston during the DISCOVER-AQ (Mazzuca et al., 2016) and SHARP
565 (Ren et al., 2013) campaigns. These results, however, are limited to the examined time period
566 and location, but comparison to O_3 and NO levels at the Camp Bullis site suggests the
567 observations at UTSA are typical for an area downwind of the San Antonio urban center. This is
568 in contrast, however, to observations at the TCEQ Pecan Valley site which has not had an ozone
569 exceedance day by either EPA standard since 2015 but regularly has MDA8 NO greater than 50
570 ppbv, significantly larger than the maximum 2-minute value of 4 ppbv seen at the UTSA site.
571 Mixing ratios of O_X at Pecan Valley and Camp Bullis (Fig. 1) are essentially identical,
572 suggesting that there is less O_3 titration downwind of central San Antonio than in the urban core.
573 Given the higher [NO_X] in the urban core of San Antonio, P(O_3) could be significantly different
574 than at the UTSA site. Supporting this idea of variations in ozone production across the San
575 Antonio region is the time series of O_3 at Pecan Valley, UTSA, and Lake Calaveras during SAFS
576 (Fig. S5). Ozone concentrations are frequently lower at this site than at both UTSA and Lake
577 Calaveras, despite its location downwind of Lake Calaveras.
578 OH reactivity at UTSA was found to be 12 s^{-1}, with the primary contributor being
579 isoprene. While the overall magnitude of the reactivity was comparable to that observed and
580 modeled during the TRAMP2006 campaign in Houston (Mao et al., 2010), the contributors to
581 OH reactivity were found to be significantly different. Contributions from aromatics were
582 negligible at UTSA while they were found to be 15% during TRAMP2006. In Houston,
583 anthropogenic alkenes were found to be responsible for 20-30% of total reactivity, with biogenic
584 VOCs making up less than 10%. Here, biogenic VOCs were responsible for 55% of total
585 daytime reactivity, with alkenes making up less than 1%, although alkene values were based on

586 estimates from a different site. We caution that this result cannot necessarily be extrapolated to
587 other areas in the San Antonio region. Isoprene has a lifetime on the order of an hour, and the
588 high biogenic contribution to OH reactivity seen here could result from local influences. While
589 there are trees throughout the San Antonio region, the results at UTSA cannot be extrapolated to
590 areas with far less foliage without further observations. Other VOCs could comprise a larger
591 fraction of total OH reactivity in less vegetated areas.

592 While the isoprene concentration at Floresville was significantly lower than at UTSA, it
593 was still the dominant contributor to OH reactivity during the afternoon, although the total OH
594 reactivity was a factor of 3 lower at this site (4 s^{-1}) than at UTSA. Schade and Roest (2016)
595 found a significantly different OH reactivity profile at Floresville than described here, with
596 alkanes accounting for approximately 70% of total OH reactivity, with biogenic VOCs
597 contributing less than 5%. Observed isoprene at Floresville during SAFS was more than an order
598 of magnitude larger than that reported in Schade and Roest (2016), with alkane concentrations
599 consistent between the two studies. When the data used in Schade and Roest (2016) are subset to
600 afternoon times and May through July, the contribution of isoprene to VOC reactivity increases
601 to a median value of 38%, in agreement with the results presented here (Schade, personal
602 communication). The differences between the two studies do suggest that there could be
603 significant seasonal and diurnal variations in OH reactivity. Nevertheless, these results suggest
604 that policies designed to limit O_3 production at the SAFS sites discussed here should initially
605 focus primarily on NO_X reductions as the region is NO_X limited and the primary VOC
606 contributor is biogenic. Further observations and analysis are need to determine whether this
607 holds true in the urban core of downtown San Antonio.

608 ***5. Data Availability***
609

Data from SAFS are maintained on a private server but are available upon request to the authors.

6. Author Contributions

D.CA. and E.W wrote the manuscript. All authors discussed the results and commented on the manuscript. All authors also contributed to daily running of the AML. S.C.H. led the campaign. D.C.A., J.P, and E.C.W. measured XO_2. B.M.L. and W.B.K. contributed to the measurement of organic trace gases. J.R.R., T.I.Y., and S.C.H. led observations with TILDAS instruments as well as measurements of NO, NO_2, and O_3.

7. Competing Interests

The authors declare no competing interests.

8. Acknowledgements

The authors acknowledge support from NSF grants AGS-1443842 and AGS-1719918. In addition, this research was funded by a grant (project 17-032) from the Texas Air Quality Research Program (AQRP) at the University of Texas Austin through the Texas Emission Reduction Program (TERP) and the Texas Commission on Environmental Quality (TCEQ). The findings, opinions, and conclusions are the work of the authors and do not necessarily represent the findings, opinions, or conclusions of the AQRP or the TCEQ. The authors thank S. Hall and K. Ullmann of NCAR, J. Flynn of the University of Houston, D. Sullivan of the University of Texas at Austin, and R. Nadkarni and M. Estes of TCEQ for their contributions to the SAFS campaign and this paper.

9. References

Bell, M. L., Peng, R. D., and Dominici, F.: The exposure-response curve for ozone and risk of mortality and the adequacy of current ozone regulations, Environmental Health Perspectives, 114, 532-536, 10.1289/ehp.8816, 2006.

Bucsela, E. J., Krotkov, N. A., Celarier, E. A., Lamsal, L. N., Swartz, W. H., Bhartia, P. K., Boersma, K. F., Veefkind, J. P., Gleason, J. F., and Pickering, K. E.: A new stratospheric and tropospheric NO_2 retrieval algorithm for nadir-viewing satellite instruments: applications to OMI, Atmos. Meas. Tech., 6, 2607-2626, 10.5194/amt-6-2607-2013, 2013.

Choi, Y., and Souri, A. H.: Chemical condition and surface ozone in large cities of Texas during the last decade: Observational evidence from OMI, CAMS, and model analysis, Remote Sensing of Environment, 168, 90-101, 10.1016/j.rse.2015.06.026, 2015.

Cooper, O. R., Gao, R.-S., Tarasick, D., Leblanc, T., and Sweeney, C.: Long-term ozone trends at rural ozone monitoring sites across the United States, 1990-2010, Journal of Geophysical Research: Atmospheres, 117, n/a-n/a, 10.1029/2012jd018261, 2012.

Duncan, B. N., Yoshida, Y., Olson, J. R., Sillman, S., Martin, R. V., Lamsal, L., Hu, Y., Pickering, K. E., Retscher, C., Allen, D. J., and Crawford, J. H.: Application of OMI observations to a space-based indicator of NO_X and VOC controls on surface ozone formation, Atmospheric Environment, 44, 2213-2223, 10.1016/j.atmosenv.2010.03.010, 2010.

Duncan, B. N., Lamsal, L. N., Thompson, A. M., Yoshida, Y., Lu, Z. F., Streets, D. G., Hurwitz, M. M., and Pickering, K. E.: A space-based, high-resolution view of notable changes in urban NO_X pollution around the world (2005-2014), Journal of Geophysical Research-Atmospheres, 121, 976-996, 10.1002/2015jd024121, 2016.

EPA: National Ambient Air Quality Standards for Ozone, Federal Register, 80, 2015.

Faloona, I. C., Tan, D., Lesher, R. L., Hazen, N. L., Frame, C. L., SImpas, J. B., Harder, G., Martinez, M., Di Carlo, P., Ren, X., and Brune, W. H.: A Laser-induced Fluorescence Instrument for Detecting Tropospheric OH and HO_2: Characteristics and Calibration, Journal of Atmospheric Chemistry, 47, 139-167, 2004.

González Abad, G., Liu, X., Chance, K., Wang, H., Kurosu, T. P., and Suleiman, R.: Updated Smithsonian Astrophysical Observatory Ozone Monitoring Instrument (SAO OMI) formaldehyde retrieval, Atmospheric Measurement Techniques, 8, 19-32, 10.5194/amt-8-19-2015, 2015.

He, H., Stehr, J. W., Hains, J. C., Krask, D. J., Doddridge, B. G., Vinnikov, K. Y., Canty, T. P., Hosley, K. M., Salawitch, R. J., Worden, H. M., and Dickerson, R. R.: Trends in emissions and concentrations of air pollutants in the lower troposphere in the Baltimore/Washington airshed from 1997 to 2011, Atmospheric Chemistry and Physics, 13, 7859-7874, 10.5194/acp-13-7859-2013, 2013.

Herndon, S. C., Jayne, J. T., Zahniser, M. S., Worsnop, D. R., Knighton, B., Alwine, E., Lamb, B. K., Zavala, M., Nelson, D. D., McManus, J. B., Shorter, J. H., Canagaratna, M. R., Onasch, T. B., and Kolb, C. E.: Characterization of urban pollutant emission fluxes and ambient concentration distributions using a

675 mobile laboratory with rapid response instrumentation, Faraday Discussions, 130, 327-339,
676 10.1039/b500411j, 2005.

677 Holton, J. R., Haynes, P. H., McIntyre, M. E., Douglass, A. R., Rood, R. B., and Pfister, L.: Stratosphere-
678 Troposphere Exchange, Reviews of Geophysics, 33, 403-439, 1995.

679 Jerrett, M., Burnett, R. T., Pope, C. A., Ito, K., Thurston, G., Krewski, D., Shi, Y. L., Calle, E., and Thun,
680 M.: Long-Term Ozone Exposure and Mortality, New England Journal of Medicine, 360, 1085-1095,
681 10.1056/NEJMoa0803894, 2009.

682 Kebabian, P. L., Herndon, S. C., and Freedman, A.: Detection of Nitrogen Dioxide by Cavity Attenuated
683 Phase Shift Spectroscopy, Analytical Chemistry, 77, 724-728, 10.1029/, 2005.

684 Kebabian, P. L., Wood, E. C., Herndon, S. C., and Freedman, A.: A Practical Alternative to
685 Chemiluminescence-Based Detection of Nitrogen Dioxide: Cavity Attenuated Phase Shift Spectroscopy,
686 Environmental Science & Technology, 42, 6040-6045, 2008.

687 Kleinman, L. I.: Low and High NO_X Tropospheric Chemistry, Journal of Geophysical Research-
688 Atmospheres, 99, 16831-16838, 10.1029/94jd01028, 1994.

689 Kleinman, L. I., Daum, P. H., Imre, D., Lee, Y. N., Nunnermacker, L. J., Springston, S. R., Weinstein-
690 Lloyd, J., and Rudolph, J.: Ozone production rate and hydrocarbon reactivity in 5 urban areas: A cause of
691 high ozone concentration in Houston, Geophysical Research Letters, 29, 105-101-105-104,
692 10.1029/2001gl014569, 2002.

693 Kleinman, L. I.: The dependence of tropospheric ozone production rate on ozone precursors, Atmospheric
694 Environment, 39, 575-586, 10.1016/j.atmosenv.2004.08.047, 2005.

695 Krotkov, N. A., Lamsal, L. N., Celarier, E. A., Swartz, W. H., Marchenko, S. V., Bucsela, E. J., Chan, K.
696 L., Wenig, M., and Zara, M.: The version 3 OMI NO_2 standard product, Atmospheric Measurement
697 Techniques, 10, 3133-3149, 10.5194/amt-10-3133-2017, 2017.

698 Kundu, S., Deming, B. L., Lew, M. M., Bottorff, B. P., Rickly, P., Stevens, P. S., Dusanter, S., Sklaveniti,
699 S., Leonardis, T., Locoge, N., and Wood, E. C.: Peroxy Radical Measurements by Ethane – Nitric Oxide
700 Chemical Amplification and Laser-Induced Fluorescence/Fluorescence Assay by Gas Expansion during
701 the IRRONIC field campaign in a Forest in Indiana, Atmos. Chem. Phys. Discuss., 2019, 1-31,
702 10.5194/acp-2018-1359, 2019.

703 Lamarque, J. F., Hess, P., Emmons, L., Buja, L., Washington, W., and Granier, C.: Tropospheric ozone
704 evolution between 1890 and 1990, Journal of Geophysical Research-Atmospheres, 110,
705 10.1029/2004jd005537, 2005.

706 Lamsal, L. N., Duncan, B. N., Yoshida, Y., Krotkov, N. A., Pickering, K. E., Streets, D. G., and Lu, Z. F.:
707 U.S. NO2 trends (2005-2013): EPA Air Quality System (AQS) data versus improved observations from
708 the Ozone Monitoring Instrument (OMI), Atmospheric Environment, 110, 130-143,
709 10.1016/j.atmosenv.2015.03.055, 2015.

710 Lee, B. H., Wood, E. C., Herndon, S. C., Lefer, B. L., Luke, W. T., Brune, W. H., Nelson, D. D.,
711 Zahniser, M. S., and Munger, J. W.: Urban measurements of atmospheric nitrous acid: A caveat on the
712 interpretation of the HONO photostationary state, Journal of Geophysical Research: Atmospheres, 118,
713 12,274-212,281, 10.1002/2013jd020341, 2013.

Mao, J. Q., Ren, X., Chen, S., Brune, W. H., Chen, Z., Martinez, M., Harder, H., Lefer, B., Rappenglück, B., Flynn, J., and Leuchner, M.: Atmospheric oxidation capacity in the summer of Houston 2006: Comparison with summer measurements in other metropolitan studies, Atmospheric Environment, 44, 4107-4115, 10.1016/j.atmosenv.2009.01.013, 2010.

Mazzuca, G. M., Ren, X., Loughner, C. P., Estes, M., Crawford, J. H., Pickering, K. E., Weinheimer, A. J., and Dickerson, R. R.: Ozone production and its sensitivity to NO_X and VOCs: results from the DISCOVER-AQ field experiment, Houston 2013, Atmospheric Chemistry and Physics, 16, 14463-14474, 10.5194/acp-16-14463-2016, 2016.

McManus, J. B., Zahniser, M. S., Nelson, D. D., Shorter, J. H., Herndon, S. C., Jervis, D., Agnese, M., McGovern, R., Yacovitch, T. I., and Roscioli, J. R.: Recent progress in laser-based trace gas instruments: performance and noise analysis, Applied Physics B-Lasers and Optics, 119, 203-218, 10.1007/s00340-015-6033-0, 2015.

Mihele, C. M., and Hastie, D. R.: Optimized operation and calibration procedures for radical amplifier-type detectors, Journal of Atmospheric and Oceanic Technology, 17, 788-794, 10.1175/1520-0426(2000)017<0788:Ooacpf>2.0.Co;2, 2000.

Orlando, J. J., and Tyndall, G. S.: Laboratory studies of organic peroxy radical chemistry: an overview with emphasis on recent issues of atmospheric significance, Chemical Society Reviews, 41, 6294-6317, 10.1039/c2cs35166h, 2012.

Park, S. K., O'Neill, M. S., Vokonas, P. S., Sparrow, D., and Schwartz, J.: Effects of air pollution on heart rate variability: The VA Normative Aging Study, Environmental Health Perspectives, 113, 304-309, 10.1289/ehp.7447, 2005.

Pollack, I. B., Ryerson, T. B., Trainer, M., Parrish, D. D., Andrews, A. E., Atlas, E. L., Blake, D. R., Brown, S. S., Commane, R., Daube, B. C., de Gouw, J. A., Dubé, W. P., Flynn, J., Frost, G. J., Gilman, J. B., Grossberg, N., Holloway, J. S., Kofler, J., Kort, E. A., Kuster, W. C., Lang, P. M., Lefer, B., Lueb, R. A., Neuman, J. A., Nowak, J. B., Novelli, P. C., Peischl, J., Perring, A. E., Roberts, J. M., Santoni, G., Schwarz, J. P., Spackman, J. R., Wagner, N. L., Warneke, C., Washenfelder, R. A., Wofsy, S. C., and Xiang, B.: Airborne and ground-based observations of a weekend effect in ozone, precursors, and oxidation products in the California South Coast Air Basin, Journal of Geophysical Research: Atmospheres, 117, n/a-n/a, 10.1029/2011jd016772, 2012.

Pollmann, J., Helmig, D., Hueber, J., Tanner, D., and Tans, P. P.: Evaluation of solid adsorbent materials for cryogen-free trapping - gas chromatographic analysis of atmospheric C2-C6 non-methane hydrocarbons, Journal of Chromatography A, 1134, 1-15, 10.1016/j.chroma.2006.08.050, 2006.

Ren, X., van Duin, D., Cazorla, M., Chen, S., Mao, J., Zhang, L., Brune, W. H., Flynn, J. H., Grossberg, N., Lefer, B. L., Rappenglück, B., Wong, K. W., Tsai, C., Stutz, J., Dibb, J. E., Thomas Jobson, B., Luke, W. T., and Kelley, P.: Atmospheric oxidation chemistry and ozone production: Results from SHARP 2009 in Houston, Texas, Journal of Geophysical Research: Atmospheres, 118, 5770-5780, 10.1002/jgrd.50342, 2013.

Ring, A. M., Canty, T. P., Anderson, D. C., Vinciguerra, T. P., He, H., Goldberg, D. L., Ehrman, S. H., Dickerson, R. R., and Salawitch, R. J.: Evaluating commercial marine emissions and their role in air quality policy using observations and the CMAQ model, Atmospheric Environment, 173, 96-107, 10.1016/j.atmosenv.2017.10.037, 2018.

Ryerson, T. B., Trainer, M., Angevine, W. M., Brock, C. A., Dissly, R. W., Fehsenfeld, F. C., Frost, G. J., Goldan, P. D., Holloway, J. S., Hubler, G., Jakoubek, R. O., Kuster, W. C., Neuman, J. A., Nicks, D. K., Parrish, D. D., Roberts, J. M., Sueper, D. T., Atlas, E. L., Donnelly, S. G., Flocke, F., Fried, A., Potter, W. T., Schauffler, S., Stroud, V., Weinheimer, A. J., Wert, B. P., Wiedinmyer, C., Alvarez, R. J., Banta, R. M., Darby, L. S., and Senff, C. J.: Effect of petrochemical industrial emissions of reactive alkenes and NOx on tropospheric ozone formation in Houston, Texas, Journal of Geophysical Research-Atmospheres, 108, 10.1029/2002jd003070, 2003.

Sanchez, J., Tanner, D. J., Chen, D., Huey, L. G., and Ng, N. L.: A new technique for the direct detection of HO_2 radicals using bromide chemical ionization mass spectrometry (Br-CIMS): initial characterization, Atmospheric Measurement Techniques, 9, 3851-3861, 10.5194/amt-9-3851-2016, 2016.

Sanders, S. P., Friedl, R. R., Abbatt, J. P. D., Barker, J. R., Burkholder, J. B., Golden, D. M., Kolb, C. E., Kurylo, M. J., Moortgat, G. K., Wine, P. H., R.E., H., and Orkin, V. L.: Chemical Kinetics and Photochemical Data for Use in Atmopsheric Studies, 2011.

Schade, G. W., and Roest, G.: Analysis of non-methane hydrocarbon data from a monitoring station affected by oil and gas development in the Eagle Ford shale, Texas, Elementa: Science of the Anthropocene, 4, 10.12952/journal.elementa.000096, 2016.

Schroeder, J. R., Crawford, J. H., Fried, A., Walega, J., Weinheimer, A., Wisthaler, A., Müller, M., Mikoviny, T., Chen, G., Shook, M., Blake, D. R., and Tonnesen, G. S.: New insights into the column CH_2O/NO_2 ratio as an indicator of near-surface ozone sensitivity, Journal of Geophysical Research: Atmospheres, 10.1002/2017jd026781, 2017.

Shetter, R. E., Junkermann, W., Swartz, W. H., Frost, G. J., Crawford, J. H., Lefer, B. L., Barrick, J. D., Hall, S. R., Hofzumahaus, A., Bais, A., Calvert, J. G., Cantrell, C. A., Madronich, S., Muller, M., Kraus, A., Monks, P. S., Edwards, G. D., McKenzie, R., Johnston, P., Schmitt, R., Griffioen, E., Krol, M., Kylling, A., Dickerson, R. R., Lloyd, S. A., Martin, T., Gardiner, B., Mayer, B., Pfister, G., Roth, E. P., Koepke, P., Ruggaber, A., Schwander, H., and van Weele, M.: Photolysis frequency of NO_2: Measurement and modeling during the International Photolysis Frequency Measurement and Modeling Intercomparison (IPMMI), Journal of Geophysical Research-Atmospheres, 108, 10.1029/2002jd002932, 2003.

Silva, R. A., West, J. J., Zhang, Y., Anenberg, S. C., Lamarque, J.-F., Shindell, D. T., Collins, W. J., Dalsoren, S., Faluvegi, G., Folberth, G., Horowitz, L. W., Nagashima, T., Naik, V., Rumbold, S., Skeie, R., Sudo, K., Takemura, T., Bergmann, D., Cameron-Smith, P., Cionni, I., Doherty, R. M., Eyring, V., Josse, B., MacKenzie, I. A., Plummer, D., Righi, M., Stevenson, D. S., Strode, S., Szopa, S., and Zeng, G.: Global premature mortality due to anthropogenic outdoor air pollution and the contribution of past climate change, Environmental Research Letters, 8, 034005, 10.1088/1748-9326/8/3/034005, 2013.

Sommariva, R., Brown, S. S., Roberts, J. M., Brookes, D. M., Parker, A. E., Monks, P. S., Bates, T. S., Bon, D., de Gouw, J. A., Frost, G. J., Gilman, J. B., Goldan, P. D., Herndon, S. C., Kuster, W. C., Lerner, B. M., Osthoff, H. D., Tucker, S. C., Warneke, C., Williams, E. J., and Zahniser, M. S.: Ozone production in remote oceanic and industrial areas derived from ship based measurements of peroxy radicals during TexAQS 2006, Atmospheric Chemistry and Physics, 11, 2471-2485, 10.5194/acp-11-2471-2011, 2011.

Stark, H., Lerner, B. M., Schmitt, R., Jakoubek, R., Williams, E. J., Ryerson, T. B., Sueper, D. T., Parrish, D. D., and Fehsenfeld, F. C.: Atmospheric in situ measurement of nitrate radical (NO_3) and other photolysis rates using spectroradiometry and filter radiometry, Journal of Geophysical Research-Atmospheres, 112, 10.1029/2006jd007578, 2007.

798 Thornton, J. A.: Ozone production rates as a function of NO_X abundances and HO_X production rates in the
799 Nashville urban plume, Journal of Geophysical Research, 107, 10.1029/2001jd000932, 2002.

800 Whalley, L. K., Stone, D., Dunmore, R., Hamilton, J., Hopkins, J. R., Lee, J. D., Lewis, A. C., Williams,
801 P., Kleffmann, J., Laufs, S., Woodward-Massey, R., and Heard, D. E.: Understanding in situ ozone
802 production in the summertime through radical observations and modelling studies during the Clean air for
803 London project (ClearfLo), Atmospheric Chemistry and Physics, 18, 2547-2571, 10.5194/acp-18-2547-
804 2018, 2018.

805 Wolfe, G. M., Kaiser, J., Hanisco, T. F., Keutsch, F. N., de Gouw, J. A., Gilman, J. B., Graus, M., Hatch,
806 C. D., Holloway, J., Horowitz, L. W., Lee, B. H., Lerner, B. M., Lopez-Hilifiker, F., Mao, J., Marvin, M.
807 R., Peischl, J., Pollack, I. B., Roberts, J. M., Ryerson, T. B., Thornton, J. A., Veres, P. R., and Warneke,
808 C.: Formaldehyde production from isoprene oxidation across NO_X regimes, Atmospheric Chemistry and
809 Physics, 16, 2597-2610, 10.5194/acp-16-2597-2016, 2016a.

810 Wolfe, G. M., Marvin, M. R., Roberts, S. J., Travis, K. R., and Liao, J.: The Framework for 0-D
811 Atmospheric Modeling (F0AM) v3.1, Geosci. Model Dev., 9, 3309-3319, 10.5194/gmd-9-3309-2016,
812 2016b.

813 Wood, E. C., Deming, B. L., and Kundu, S.: Ethane-Based Chemical Amplification Measurement
814 Technique for Atmospheric Peroxy Radicals, Environmental Science & Technology Letters, 4, 15-19,
815 10.1021/acs.estlett.6b00438, 2017.
816

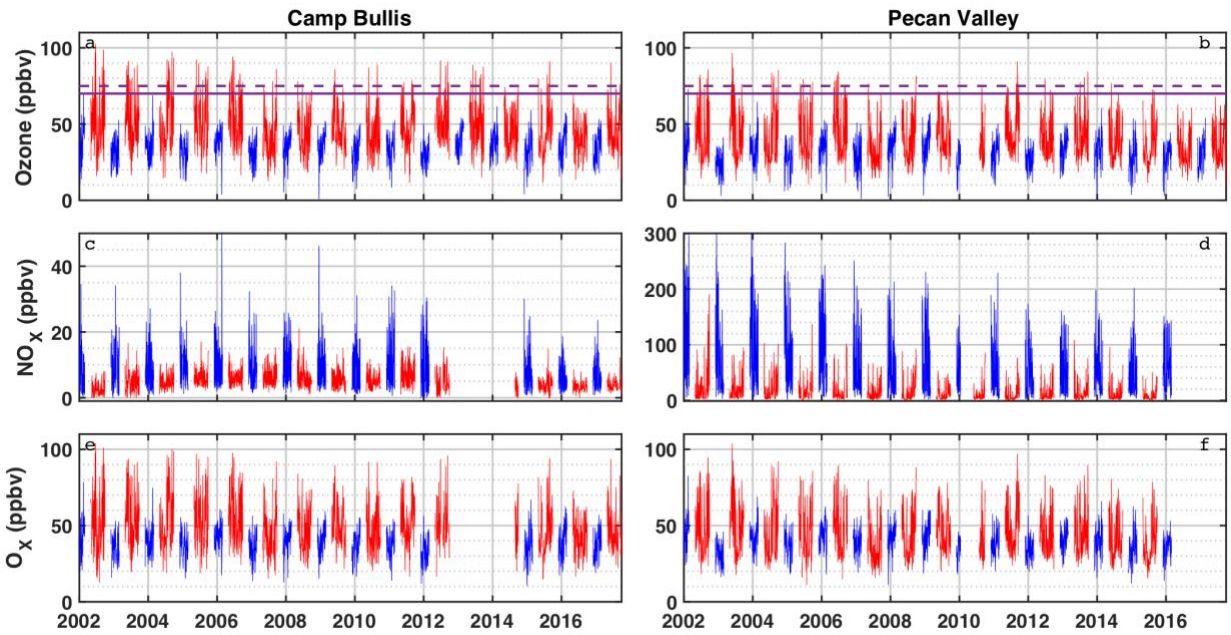

817

818 **Figure 1:** Time series of maximum daily average 8-hour (MDA8) O_3, NO_X, and O_X at the Camp
819 Bullis (**a**, **c**, **e**) and Pecan Valley (**b**, **d**, **f**) TCEQ sites for 2002 – 2017. Summer months (May –
820 September) are shown in red, and winter months (December – February) are shown in blue. MDA8
821 is calculated by determining the maximum value of a species from running 8 hour averages
822 throughout the day. The purple dashed and solid red lines represent the 2008 (75 ppbv) and 2015

(70 ppbv) O_3 standards respectively. Data were downloaded from www.tceq.texas.gov/goto/tamis.

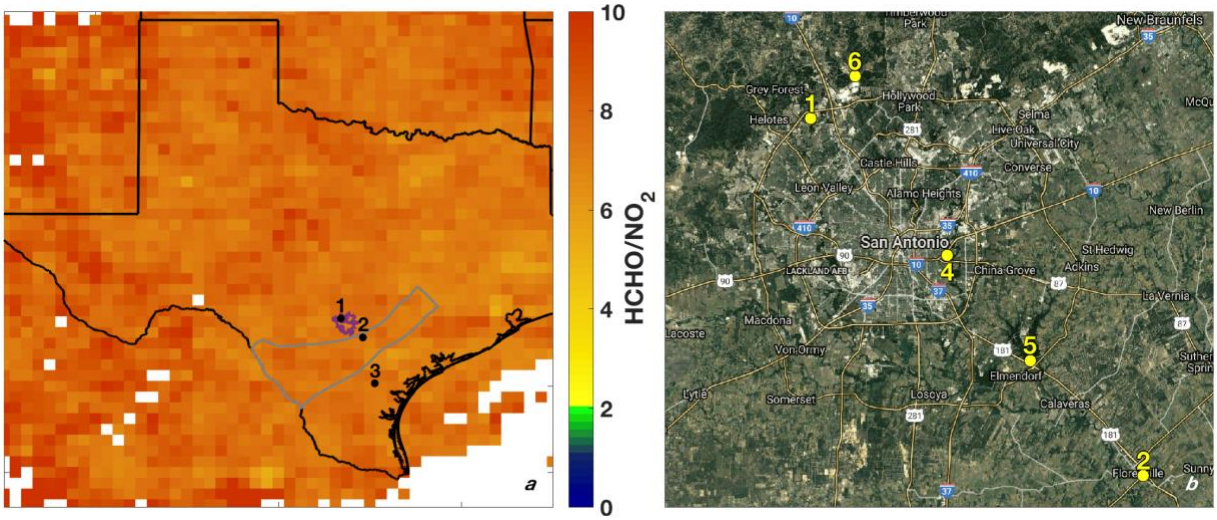

Figure 2: The sampling locations for the AML are indicated: 1 – University of Texas San Antonio, 2 – Floresville, 3 – Lake Corpus Christi. The ratio of total column HCHO to tropospheric column NO_2 averaged over the months of May through July 2017 is also shown for grid boxes with 10 or more observations of both species over the indicated time period. The outlines of the Eagle Ford Shale (grey) play and San Antonio city limits (purple) are also shown for reference. (b) The major roadways and TCEQ monitoring stations (6: Camp Bullis, 4: Pecan Valley, 5: Calaveras Lake) in the San Antonio region used in this study are shown. The UTSA and Floresville SAFS sites are also shown for reference.

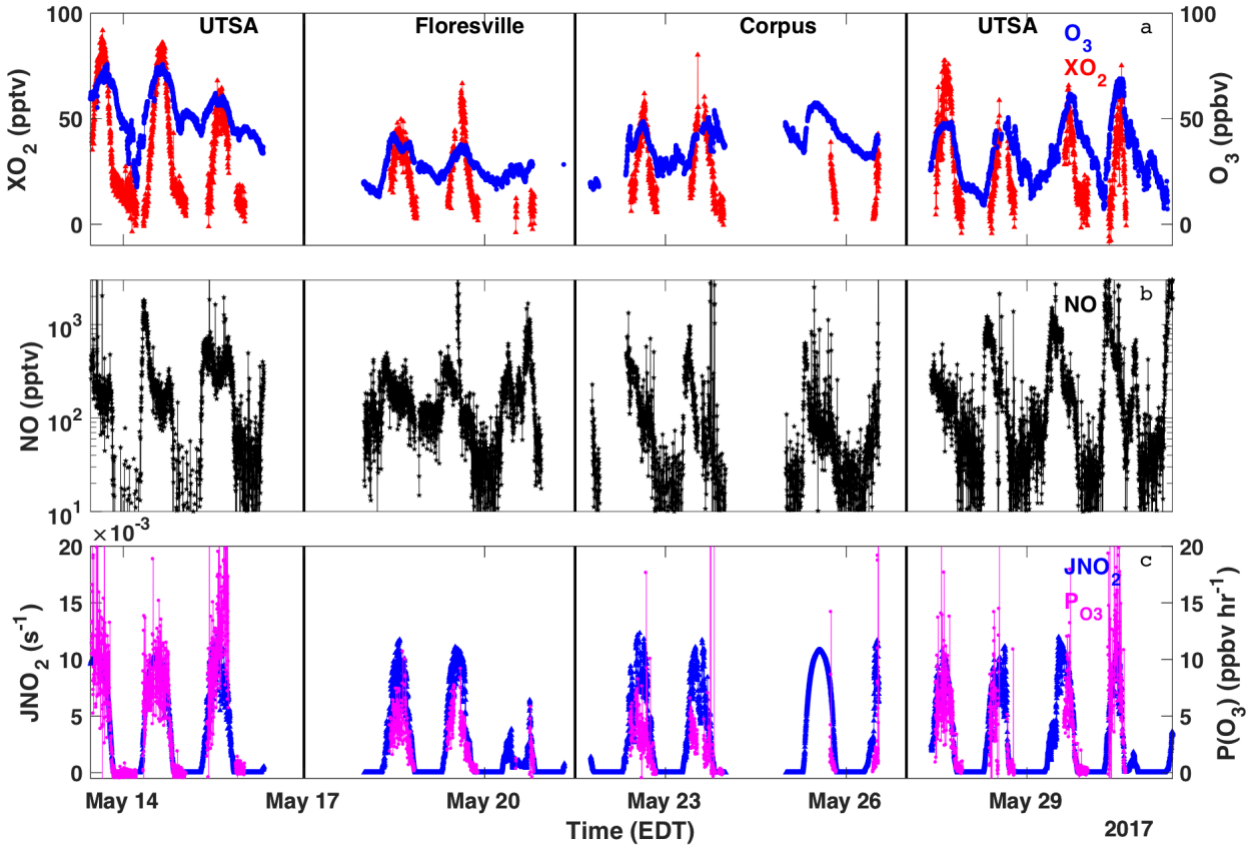

836

837 **Figure 3:** Time series of O_3 (blue circles), XO_2 (red triangles), NO (black stars), JNO_2 (blue triangles),
838 and $P(O_3)$ (magenta circles) measured at all sites. All data are averaged over the XO_2 sampling period.

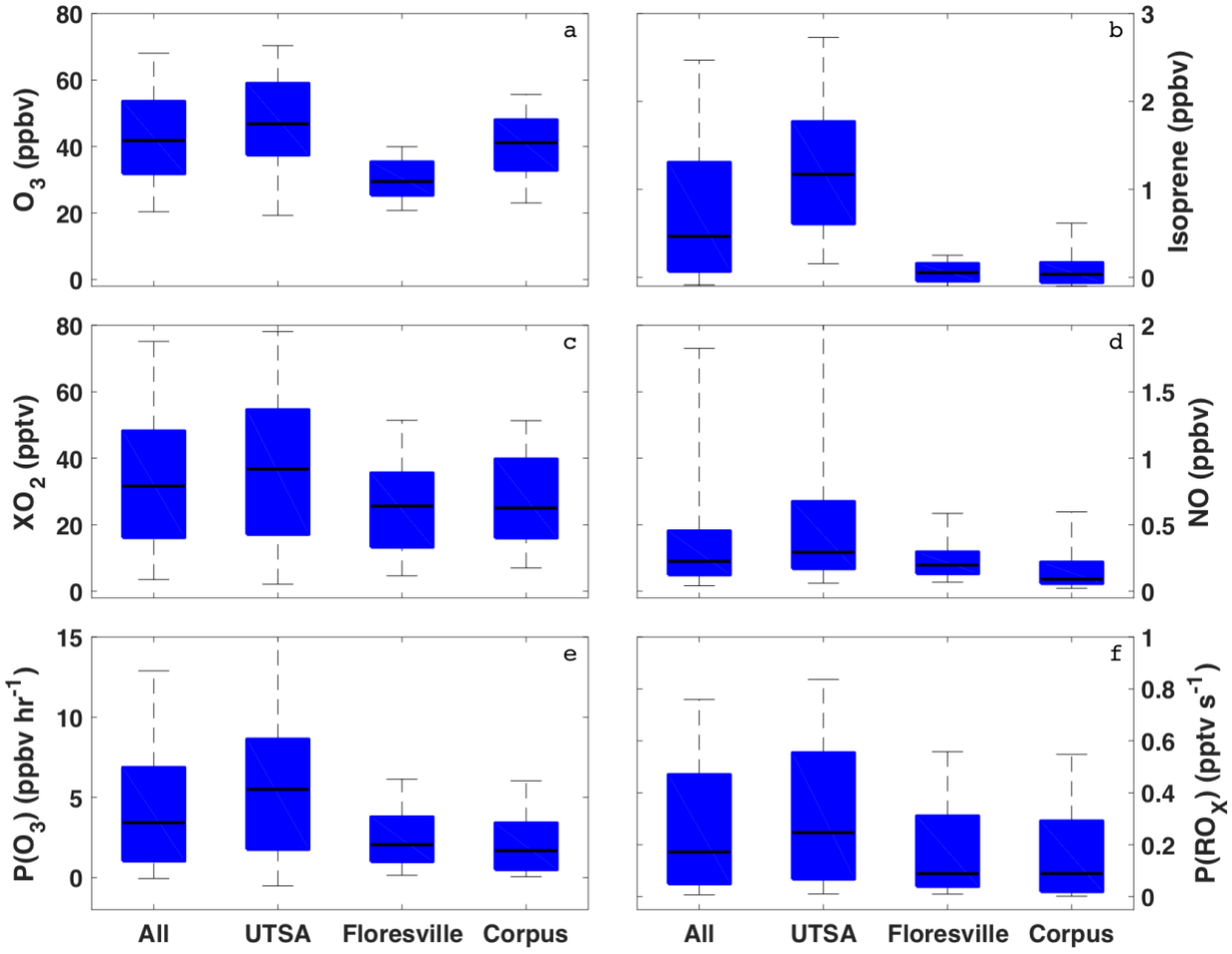

Figure 4: The distribution of O_3 (**a**), isoprene (**b**), XO_2 (**c**), NO (**d**), $P(O_3)$ (**e**), and $P(RO_X)$ (**f**) for all observations during SAFS taken between 07:00 and 20:00. The distribution for the entire campaign (All) as well as at the individual sites is shown. Medians are indicated by the black lines, and the 5^{th}, 25^{th}, 75^{th}, and 95^{th} percentiles are shown by the edges of the box and whiskers.

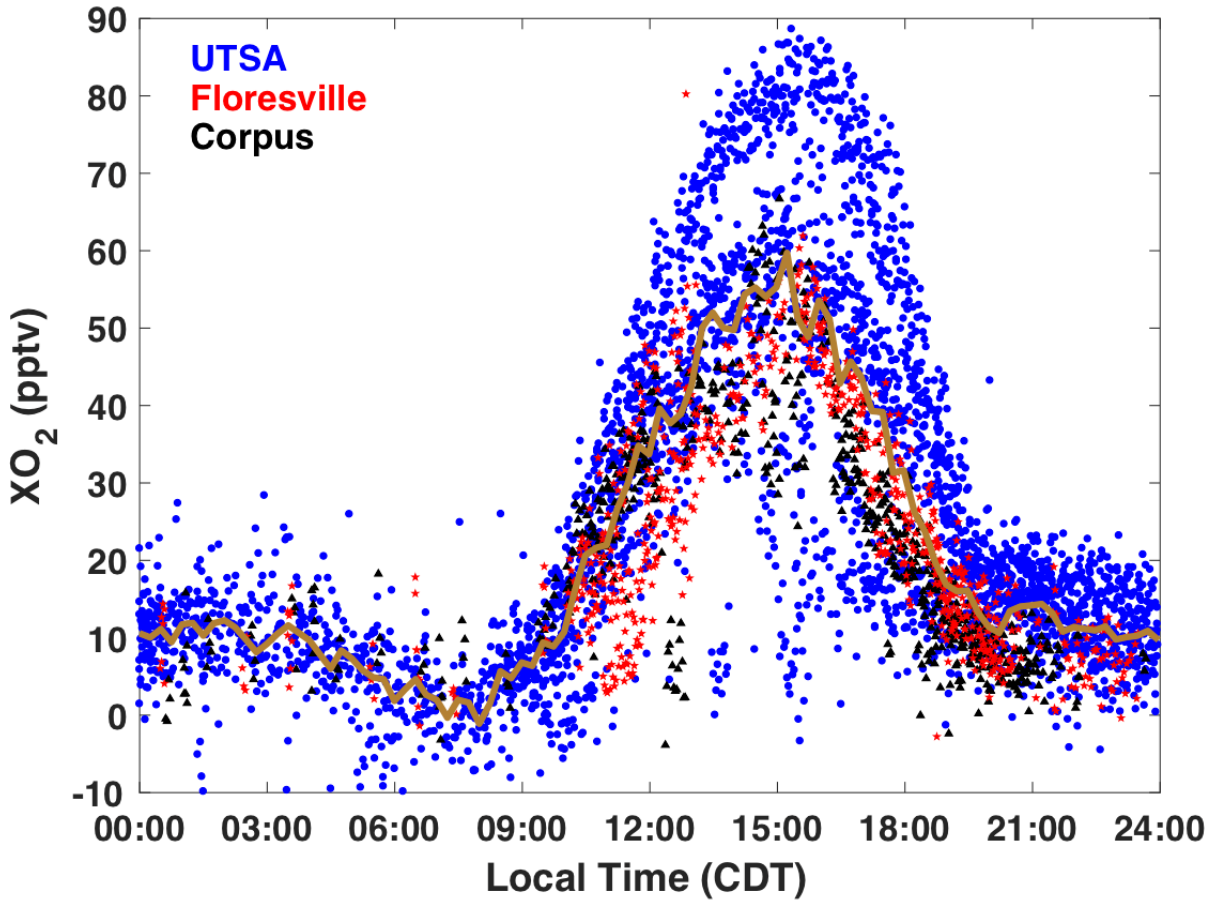

845

846 **Figure 5:** The diurnal profile of all 2 minute average XO_2 observations made during SAFS. Observations
847 made at UTSA are shown in blue, Floresville, in red, and Corpus, in black. The median value for 15-
848 minute time bins for observations at all sites is shown by the gold trace.

849
850
851
852

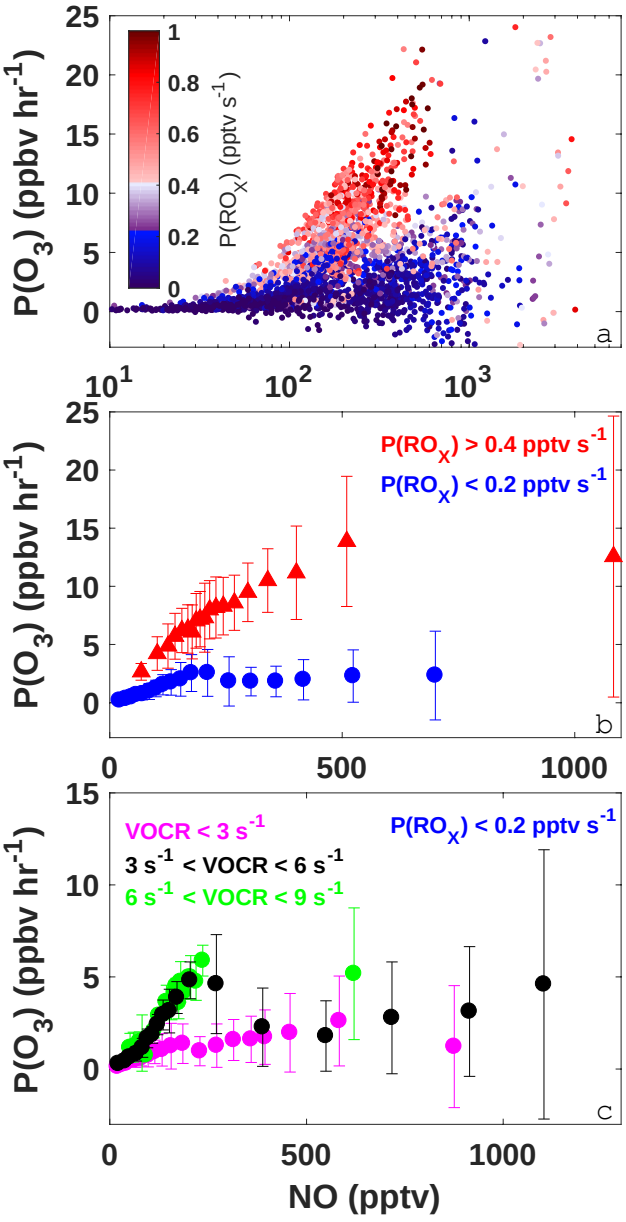

853

854 **Figure 6:** The variation of $P(O_3)$ with NO for all daytime observations (07:00 to 20:00) made during
855 SAFS (**a**). Observations are colored by $P(RO_X)$. The same data as shown in panel (**a**) but sorted by
856 $P(RO_X)$ are shown in panel (**b**). Observations with $P(RO_X)$ greater than 0.4 pptv s^{-1} are shown in red,
857 while observations with $P(RO_X)$ less than 0.2 pptv s^{-1} are shown in blue. Data are separated into NO bins
858 with an equal number of observations per bin. The mean value of each bin is shown, with the error bars
859 showing one standard deviation. The subset of observations with $P(RO_X) < 0.2$ pptv s^{-1} are further
860 separated into three categories: low VOC reactivity (VOCR < 3 s^{-1}; magenta), medium VOC reactivity (3
861 < VOCR < 6 s^{-1}; black), and high VOC reactivity (6 < VOCR < 9 s^{-1}; green) (**c**). As in panel (**b**) data are
862 separated into NO bins with equal numbers of observations in each bin.

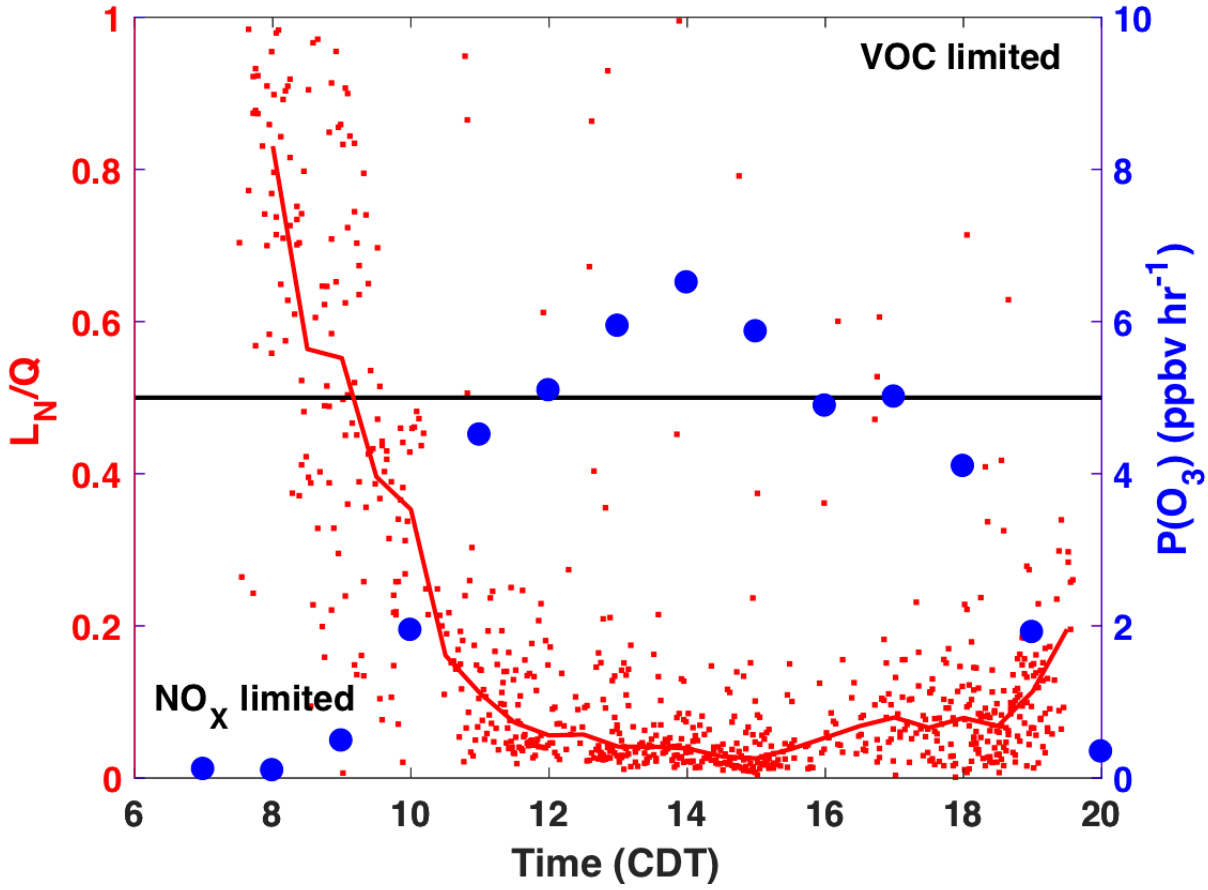

Figure 7: The diurnal profiles of L_N/Q calculated with the F0AM box model (red), and the median $P(O_3)$ in one hour time bins (blue). The median L_N/Q value for half hour bins is shown by the red line. Profiles are only for observations at UTSA. Points are calculated by $P(O_3)$ calculated from observations. The black line is approximately the separation between the NO_X- and VOC-limited regimes.

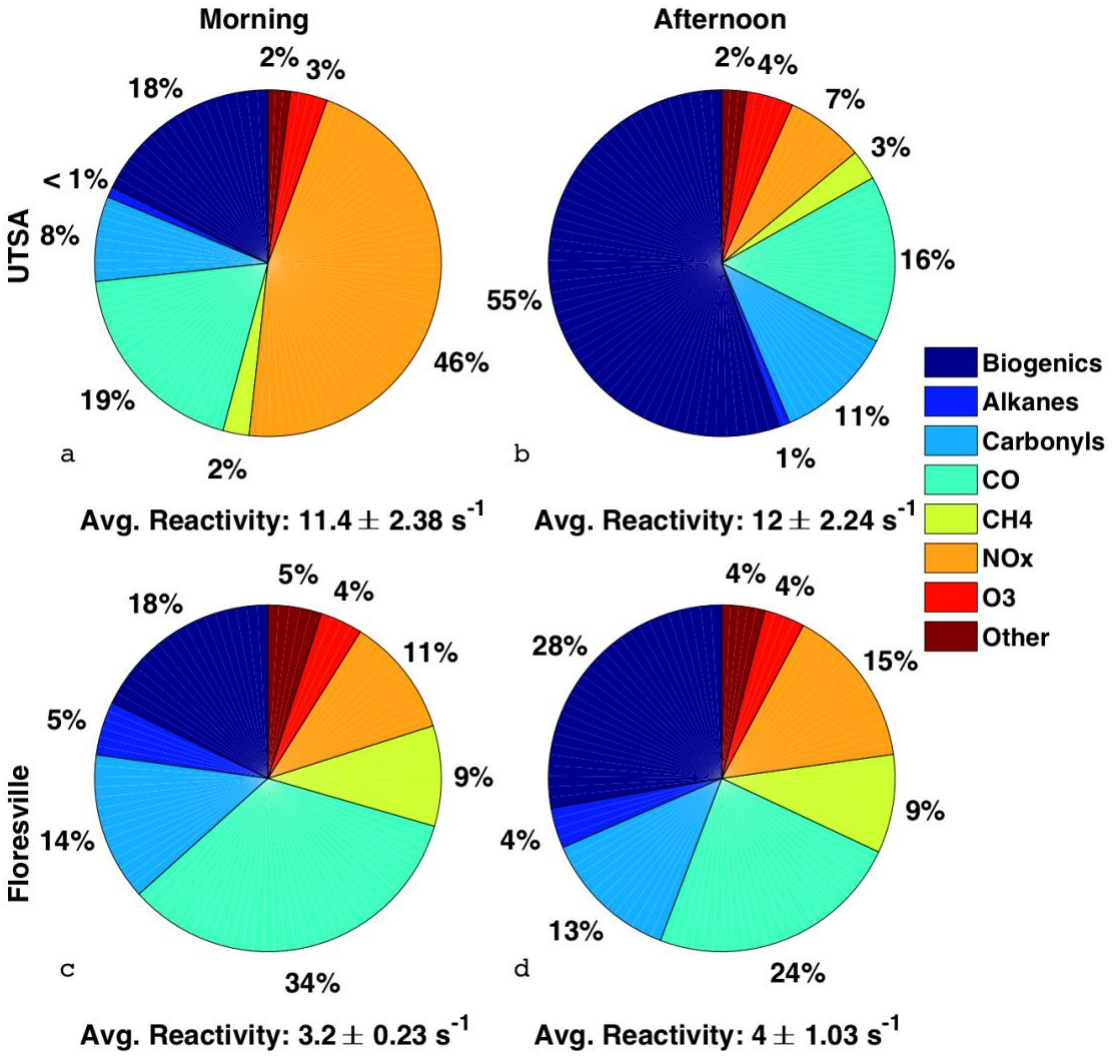

Figure 8: The distribution of the various contributors to the overall OH reactivity for the UTSA (13 -16 May) and Floresville (17 – 19 May) sites are shown for both the morning, times between 7:00 and 11:00, and afternoon, times between 13:00 and 20:00. The average OH reactivity (±1σ) is also shown.